Crystallization Dynamics in Model Emulsions from Magnetic Resonance Imaging

C. Simoneau, M.J. McCarthy, R.J. Kauten and J.B. German*
Food Science and Technology Department, University of California, Davis, Davis, CA 95616

Melt crystallization of trilaurin and trimyristin was investigated in the bulk and in dispersed systems using magnetic resonance imaging. Crystallization rates were studied as a function of time in fat/water (40:60) emulsions containing 0.5% tween 80 and 0.2% xanthan gum to prevent creaming. Oil weighted images were obtained to follow the dynamics of crystallization in the bulk and in an emulsified system. Localized spectroscopy using a stimulated echo pulse sequence was used to quantify the crystallization dynamics pattern at different locations in a trimyristin emulsion (40:60). The results showed that crystallization in the emulsified state occurred over a longer period of time than in the bulk. Imaging allowed for the qualitative visualization of crystallization. Images showed crystallization occurring from the edge to the center. On the other hand, localized spectroscopy allowed for spatially quantitative measurement of the amount of liquid oil, crystalline oil and water. In the trimyristin emulsion (40:60), spectra recorded from the top, center and bottom showed a relatively abrupt crystallization pattern starting earlier at the edges of the container, as previously visualized by the images taken.

KEY WORDS: Crystallization, fats, magnetic resonance imaging, O/W emusion, triglycerides.

Crystallization of oils is a critical process in the structure and physical properties of many biomaterials, such as foods. Food stability is dictated in part by changes in the physical state of fat and crystallization processes. Lipid crystallization is also crucial in biological systems, from fat malabsorption to the formation of arteriosclerotic plaque. What has not been well characterized is the role of physical state of dispersions on crystallization and the specific triglyceride structures and physical states responsible for major fat physical properties (1).

The melting and solidification of glycerides have been well described (2,3), as has the melting range of different fats. Differential Scanning Calorimetry (DSC) studies have given an insight into the polymorphism of fats in the bulk (4,5) and in emulsions (6,7). Freeze-fracture and X-ray diffraction studies have investigated structures which can be found in liquid and crystalline fats (5,8). Finally, low-resolution nuclear magnetic resonance (NMR) provided data on the solid/liquid fat ratios (9,10). However, to a large extent, crystallization is dictated not by thermodynamics, but by the kinetics. Kinetics of crystallization is, in turn, dictated by the presence of a number of nuclei, and by the state of dispersion. The actual dynamics of the crystallization process, particularly in complex dispersions, has not been fully assessed yet. There is a lack of information on crystallization kinetics as it happens dynamically in multiphase systems. The effect of dispersion has been widely considered to have an effect on crystallization. Crystallization has been proposed to be entirely different in the bulk and in a disperse state, and the differences found have been explained by nucleation theory (7), although there is still confusion (8). Moreover, the behavior of triglycerides in large quantities, either in a multiphase system (such as cream in a tank) or in bulk may be very different than in a very small amount. Thus techniques that have proven to be useful such as DSC, freeze fracture, X-ray diffraction and NMR, may not be the most appropriate techniques for studying dynamic processes as they occur *in situ*. Since the fat structure is so important to crystallization and that the prediction of thermodynamics is not directly applicable, it is important to follow crystallization in complex systems without compromising the structure and integrity of the system.

Our overall objective was to investigate the role of the state of dispersion on crystallization. For this purpose, we sought to determine if it was possible to follow crystallization in a disperse state without compromising the structure of the system. The use of magnetic resonance imaging (MRI) for studying noninvasively dynamic processes has been mainly employed in the medical field to detect tumors and other abnormalities in humans. However, the potential of MRI for studying dynamic processes in biological materials, such as foaming or crystallization, has not been fully explored yet (11,12). Our approach was to couple relaxation time weighted imaging and localized spectroscopy to follow qualitatively and quantitatively, respectively, the progress of crystallization of triglycerides noninvasively. To achieve this goal, we focused our investigation on generating a unique signal for liquid fat separated from water.

EXPERIMENTAL PROCEDURES

Materials. The liquid oil samples consisted of glycerol tricaprate-tricaprin-, glycerol trilaurate-trilaurin-, glycerol trimyristate-trimyristin-or glycerol trioleate-triolein- (Capital City Products, Columbus, OH) containing 0.5% in volume per volume of polyoxyethylene sorbitan monooleate Tween 80 emulsifier (Sigma Chemical, St. Louis, MO) and 0.2% in volume per volume Keltrol food grade xanthan gum stabilizer (Kelco, Division of Merck & Co. Inc., Rahway, NJ). The emulsion samples consisted of triolein, tricaprin, trilaurin and trimyristin dispersed in distilled water (40:60), again containing 0.5% tween and 0.2% xanthan. Each of the triglycerides mentioned above was made into an emulsion. A water standard consisted of distilled water including 0.5% Tween 80 and 0.2% xanthan.

Triolein and tricaprin were used for MRI spectrometer calibration both as bulk and emulsion standards, against a water standard. Trilaurin and trimyristin were successively tested for their crystallization behavior in the bulk and emulsion. Samples of bulk fats were placed in an oven at 60–80°C to melt all fat to the liquid state. Water to be used in emulsion generation was also kept

*To whom correspondence should be addressed.

at that temperature. A fresh, 10-mL stock solution of bulk fat and emulsion (containing emulsifier and thickener) was made for each triglyceride to be tested and homogenized using a Brickman homogenizer at speed 5 for 30 seconds. The series of three samples of bulk fat, emulsifier fat and water standard to be tested was then immediately transferred to 5-mL, closed cylindrical glass vials. The three vials were then placed adjacent on a plexiglass sample holder into the coil positioned in the superconducting magnet.

METHODS

Magnetic resonance imaging and localized spectroscopy measurements were performed using a 2-T (General electrics, CSI) Fourier Transform imaging spectrometer tuned to the hydrogen nuclear frequency of 85.5 MHz with a 4-inch Radio Frequency (RF) imaging coil (Custom-built).

A Fourier imaging spin-echo pulse sequence was used to generate the two-dimensional images (13), and a stimulated echo (STE) pulse sequence (14) was used to generate spatially localized spectra of oil and water.

The external magnetic field was first adjusted for maximum homogeneity. This was accomplished using the standard series consisting of liquid fat, liquid fat/water emulsion (40:60) and water. The liquid fat used in this case was either triolein or tricaprin. The sample of either trilaurin or trimyristin emulsion was then put on the sample holder together with its corresponding bulk fat and water standards.

Crystallization at 20°C was followed as a function of time as corresponding images were taken. Localized spectroscopy using a STE sequence performed between images was used to obtain proton signal intensities in the different environments (solid fat, liquid fat, against water) in three spatial locations in the sample (top, bottom, and center of the emulsion respectively).

NMR theory. Proton nuclear magnetic resonance (NMR) spectroscopy is based on the ability of a hydrogen nucleus to resonate under certain conditions in the presence of a magnetic field. If an oscillating magnetic field is applied at the correct frequency, the nucleus will resonate (precess) about the equilibrium position. The frequency of the oscillating magnetic field for resonance is called the Larmor frequency ω_0 defined by the Larmor equation: $\omega_0 = -\gamma B_0$ [1], in which the Larmor frequency, ω_0, is the radiofrequency required to displace the nuclear spin from equilibrium; B_0 is the magnetic field strength, and γ is the gyromagnetic ratio which is constant for each particular nucleus.

To acquire magnetic resonance spectra, a sample is placed in an homogeneous external magnetic field, B_0 aligning the nuclear magnetic dipoles in equilibrium position. A second magnetic field, B_1, is applied as a radiofrequency (RF) pulse, causing the nuclei to enter a non-equilibrium state. Following this pulse, the excited nuclear spins give up energy to return to the equilibrium state, as they precess back to their original position at the Larmor frequency.

This relaxation of the magnetization to the equilibrium state can be characterized by two relaxation time constants. Spin-lattice relaxation, T1, is an enthalpic exchange of energy between the excited nuclear spins and their surroundings or lattice. Spin-spin relaxation, T2, describes the exchange of energy between like nuclei and can be thought of as an entropic process (15). Both time constants are important in MRI experiments, since the difference in relaxation times will be seen as a contrast in the NMR image, and as a difference in the proton signal intensity in the localized spectrum (16).

High resolution NMR spectroscopy resolves molecular structure information (17). Magnetic resonance imaging spectroscopy is an extension of standard two-dimensional NMR techniques. Information on the macroscopic spatial distribution within a sample can be provided with MRI by recording the influence of linear magnetic field gradients on the NMR signal. If a gradient is applied in the y-direction the Larmor equation becomes: $\omega_0 = -\gamma(B_0 + Gy)$ [2]. Thus, one can relate the intensity distribution in the frequency domain to a spatial location according to Equation [2].

The basis for an NMR imaging experiment is a pulse sequence, which indicates the order and timing of application of radiofrequency and gradient fields as well as signal acquisition (17). Spatially, the area of interest is referred by x, y and z coordinate axes. A pulse is applied in the presence of a magnetic gradient along one of the axes to isolate a region or slice normal to the axis along which the gradient is applied. A variable amplitude gradient applied along another axis introduces a phase variation, so that the distribution of spins can be measured. The third gradient along the remaining axis is called the read gradient. It is on when the radiofrequency receiver is on for data acquisition. A spin echo sequence such as the ones used here is based on the application of a second pulse to generate an echo during the data acquisition period. By repeating the pulse sequence several times, a magnetic resonance spectrum results. The more repetitions, the greater the signal to noise ratio. The predelay or time between two repetitions serves to reduce or enhance the effects of spin-lattice relaxation (17). A pulse sequence can be generated to produce specific information on molecular mobility, composition or velocity (17).

Image generation. The imaging experiments were based on a standard spin echo imaging pulse sequence previously described (13). In addition to the homogeneous external magnetic field, pulsed linear magnetic field gradients are applied to produce a frequency variation across the sample which can be converted into spatial coordinates. The basic radiofrequency (RF) sequence for magnetic resonance imaging using spin echo is: 90°TE/2-180°TE/2, as shown on Figure 1. A selective 90° pulse is applied in the presence of a z gradient (Gz). A Gy variable amplitude gradient introduces phase variation and the Gx gradient is the read gradient. A non-selective 180° pulse is applied to generate a spin echo.

The adjustment of the echo time (TE, the period during which sample magnetization dephases and then rephases) and predelay time (or interpulse delay) allowed T1 and/or T2 relaxation weighted image contrast (17). Enhancement of the 1H signal from the oil component was obtained using a T1 weighted spin-warp spin echo image sequence (13). Predelay and echo times were 200 ms and 21 ms, respectively, in order to obtain fat enhanced images where liquid oil shows the largest intensity, thus having the largest brightness in the image. The slice thickness was taken as 4 mm. The corresponding measur-

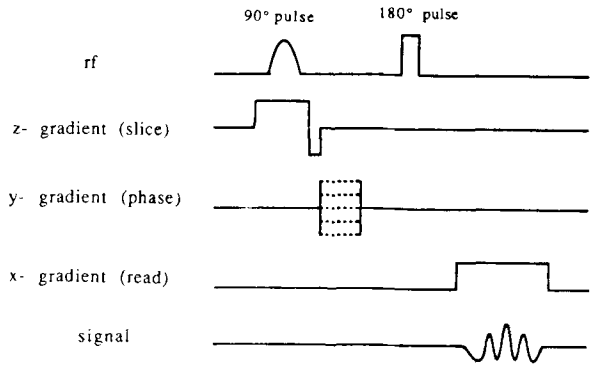

FIG. 1. Spin-echo imaging pulse sequence. The pulse sequence consists of application of a selective 90° pulse in the presence of a z-gradient (Gz) to isolate a plane normal to the z axis. A Gy gradient allows for phase encoding of nuclei along the y axis. A Gx gradient is used for frequency encoding and is referred to as the read gradient. A nonselective 180° pulse is applied to generate a spin echo during the data acquisition mode.

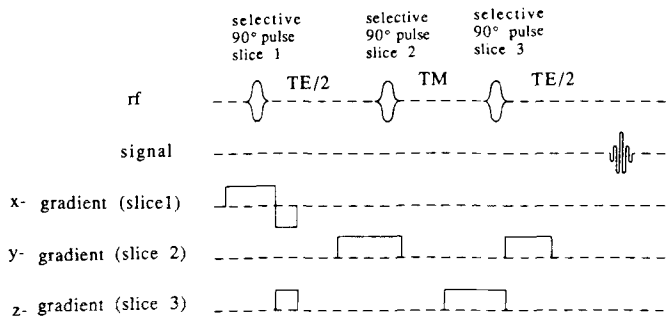

FIG. 2. Stimulated spin echo pulse sequence. The pulse sequence consists of application of three selective 90° pulses. Each pulse selects a slice, and results in selection of a volume of interest. The slice thicknesses determine the final volume element. Localization is determined from an image previously taken with the pulse sequence previously described.

ing times were 3–4 min for a 128*128 pixel image with two acquisitions. In this case, each recorded spin echo (rephased sample magnetization) is represented by 128 data sampling points, and a sum of 2 FIDs of 128 computer block memory each are added to generate the 128*128 point data matrix. In experiments using a trimyristin emulsion imaging, a 256*256 data array was used with a field of view of 50.06 mm. A magnetic resonance image results from measurement and reconstruction of the signal intensity of volume elements throughout a sample. The NMR signal from each volume element resulting from a standard spin-warp echo sequence is a function of the spin density, T1, T2 and experimental parameters (17). The predelay and the echo time are variables which can be set for each type of experiment. The signal intensity thus represents information on the density and relaxation behavior of the nuclei. In a system such as an emulsion, hydrogen nuclei from two different components (oil and water) contribute to the total signal. Differentiation between the components can be achieved using a standard spin-echo pulse sequence (18).

Spatially localized proton magnetic resonance spectroscopy. The technique utilizes the principle of slice selection in a three pulse sequence exiting three orthogonal sections (14). It consists of three slice selective radiofrequency (RF) pulses applied in the presence of orthogonal magnetic field gradients according to the following sequence: 90° (selective)-TE/2-90° (selective)-TM-90° (selective)-TE/2-.The sequence diagram is represented in Figure 2. Each one of the three slice selective pulses excites a plane of spins in one of the orthogonal gradient directions. The first pulse rotates the magnetization from the selected plane of spins to the transverse. Following free precession of the isochromats during the interval TE/2, a second slice selective 90° pulse is applied. The component of the transverse magnetization that is aligned along the y′ axis of the rotating frame of reference is stored as longitudinal magnetization and subsequently gives rise to the stimulated echo. The residual component of the transverse magnetization that is aligned along the x′ axis gives rise to a spin echo and dephases in the presence of the slice selection gradient. During the interval TM following the second 90° pulse, the longitudinal magnetization will relax by the usual spin lattice process. The longitudinal magnetization is restored to the transverse plane by the third slice selective 90° pulse and the stimulated echo is recorded as a half echo at time TE/2 later (19).

The pulse sequence used allows for the selection of a volume of interest, which resides at the intersection of the three slice planes. The STE occurring at the time, TE, is localized by the fact that only spins (protons) experiencing all three RF pulses contribute to the acquired signal. These spins originate only from the intersection of the three slices selected by the three 90°RF pulses. The position and size of the volume of interest is defined by the selectable positions and thicknesses of the individual slices. From the position of any region of interest within the field of view of the images, the appropriate offsets for each of the three orthogonal slices were calculated and supplied as parameters for the STE sequence. Figure 3 illustrates the determination of spatial coordinates to be supplied as STE parameters from the field of view of the image. The field of view was set using the spin warp imaging sequence to 50.06*50.06 mm. The very center of the image is the point of zero coordinates. Each axis goes from −25 to +25 mm, and coordinates of any spatial position can be quickly calculated. For example, parameters for the liquid fat toward the top would be X=0, Y=−3, Z=+15.

T1 and T2 relaxation times can be determined using this pulse sequence, just by varying the length o the corresponding intervals TM (middle interval time) or TE (echo time) in a series of experiments without the need of additional pulses (14). By exploiting independent adjustments of strong T1 (lipid resonance) and T2 (water resonance) weightings, both water and lipid proton signals can be obtained. This sequence could be used for suppression of such signals as well.

TE was set to 16 ms to avoid suppressing any oil or water signals having both relatively short T2 values; TM was set to 5 ms to avoid discrimination against the oil component having a short T1 value. All spectra were obtained through Fourier transformation of the original raw data. Four acquisitions were used for each spectrum

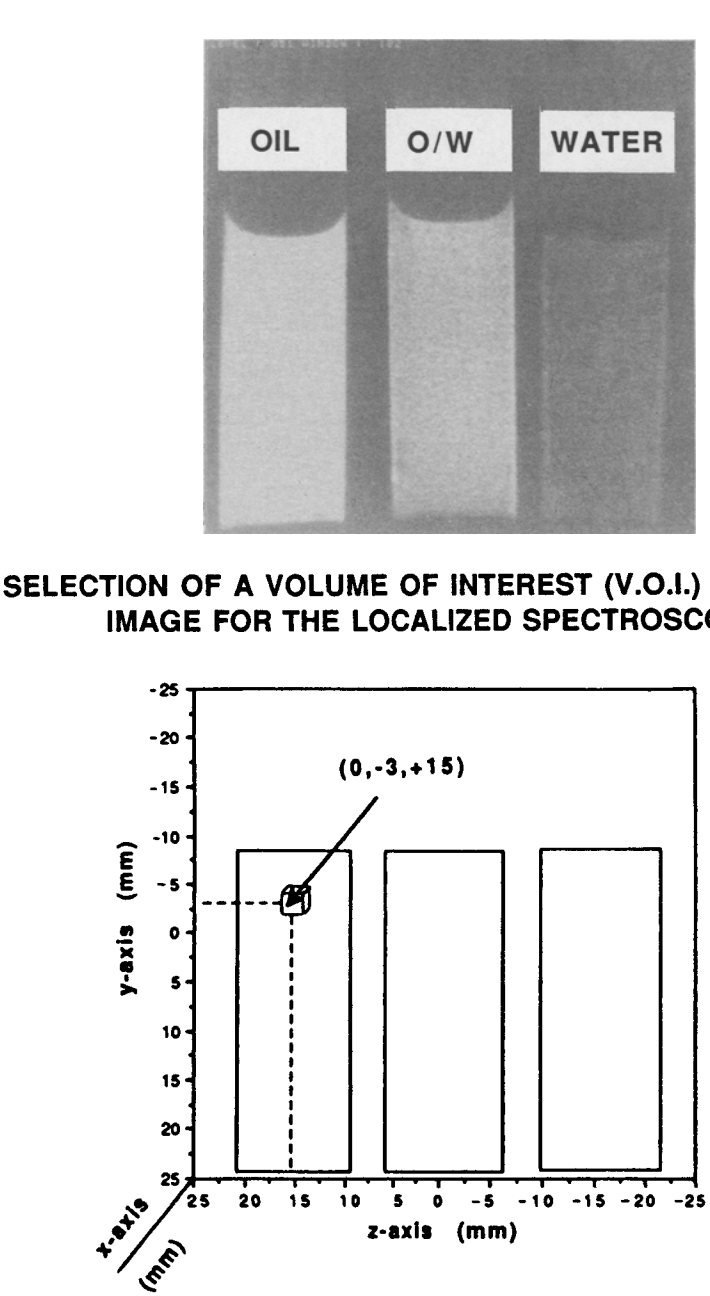

FIG. 3. Triglyceride model systems as placed in the coil. A fat weighted image of the models as placed in the coil is shown. On the left is the liquid fat, on the right is the water standard and the emulsion is placed in the middle. Having all three samples allows for determination of the image contrast based on the three components. The field of view or frame dimension of the image helps determine the coordinates to be supplied as parameters in the STE puilse sequence as illustrated. In this examkple, the arrow points to a volume located at coordinates of X=0, Y=−3, Z=+15.

generated to improve the signal to noise ratio of the resulting spectra.

RESULTS AND DISCUSSION

Our overall objective is to follow crystallization in multiphase systems. To achieve this goal it is necessary to distinguish liquid fat from solid fat from water. Thus, our first objective was to generate a separate signal for liquid fat, solid fat and water, respectively. We also needed to correlate the signal intensity in liquid and crystallized fat using imaging. For this purpose, model triglycerides were selected as a function of their capability to crystallize at 20°C in a relatively short time

frame. Triglycerides with melting points above room temperature were thus selected.

Standards of liquid fat, emulsion of liquid fat/water (40:60) and water were used for setting the MRI spectrometer for optimum magnetic field homogeneity. We observed no difference in intensity (in imaging or an oil peak) for different oils in the liquid state. Triolein was used in preliminary experiments, and since the triglyceride model systems were medium chain saturated triglycerides, tricaprin, which remains liquid during the experiments, was then chosen as a standard.

Tween 80 (0.5%) and xanthan gum (0.2%) were added to the emulsions to prevent creaming since emulsion droplets otherwise tend to rise during the time frame of these experiments (18). Since the introduction of xanthan gum as a stabilizer and Tween 80 as emulsifier changed the relaxation times of the proton as compared to relaxation times either in pure water or in pure oil, xanthan gum and Tween 80 were also included in the bulk fat and water samples.

Crystallization kinetics of triglyceride model systems in the bulk. Oil-specific proton intensity was monitored for each triglyceride in its bulk state over time. The crystallization behavior of trilaurin was assessed at 20°C. The images taken were oil weighted, so that the proton signal of the pure liquid fat appears very bright, whereas the crystallized bulk fat shows no signal at all due to fast relaxation times. Indeed, the pulse sequence used is specifically designed to provide a relaxation-specific measurement. Therefore, intensity loss of the signal is a reflection of crystallization. Crystallization of trilaurin occurring from the edge of the sample to the center can be clearly seen in Figure 4. Localized spectroscopy monitored on the bulk trilaurin over time (data not shown) showed a total disappearance of the oil peak over time.

Experiments on crystallization of trimyristin in the bulk showed that trimyristin readily crystallized and signal completely disappeared in less than 5 min. Again, the bulk fat in its crystalline form exhibited zero signal intensity.

Crystallization of model triglycerides in emulsion. Trilaurin and trimyristin were then compared at 20°C in the bulk state *vs.* the emulsified state. By placing a bulk fat and fat/water emulsion together with a water standard, we could quantitatively assess the loss in oil specific signal, hence the extent of crystallization. The water and bulk fat served as a reference for signal intensity. These experiments indeed reflected that the emulsification had a profound effect on the time required for crystallization.

Trilaurin. In contrast to trilaurin in the bulk in which the sample became fully crystallized within 2 hr, trilaurin in a 5-mL (40:60) emulsion did not crystallize within 4 hr, and not even within 2 weeks (data not shown) when placed at 20°C after an initial temperature of 70–80°C. Localized spectroscopy (data not shown) showed no difference between the spectra taken at any location within the sample as a function of time, illustrating both the lack of crystallization and the absence of creaming with Tween 80 and xanthan gum. Due to its inherent noninvasive characteristic, the technique works equally well for components which require a very long time to crystallize, since measurements can be repeated over a long period of time.

Trimyristin: Imaging. A similar emulsion of trimyristin was generated and its crystallization was followed with time under the same conditions. Again, the crystallization rate of trimyristin in a emulsion (40:60) was found to be different than in bulk. Fat enhanced images taken at various times (Fig. 5) demonstrated that the 5 mL sample was fully crystallized in 45 min, with crystallization occurring from the edge to the center. The MRI system allows for spatial resolution of crystallization in real time for multiphase samples (of various sizes).

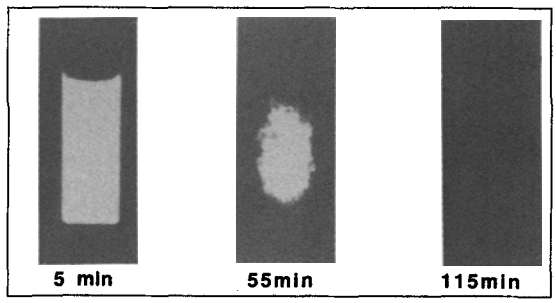

FIG. 4. Crystallization of trilaurin in the bulk. Three fat weighted images summarize cystallization of trilaurin in the bulk. The images from left to right were taken at 5, 55 and 115 min, respectively. The total disappearance of the signal corresponds to fat crystallization. Complete crystallization of trilaurin was completed in about 2 hr when placed at 20°C with an initial temperature of 70–80°C for a 5-mL volume. Crystallization of trilaurin occurred from the edge of the sample to the center.

These results obtained comparing crystallization of trimyristin or trilaurin in the bulk and in fat/water emulsion support previous results obtained on butterfat in the bulk and in emulsion through Differential Calorimetry data (7).

Correlation between imaging and localized spectroscopy. The advantage of MRI as a tool for studying any dynamics process, *e.g.*, creaming or crystallization, is that it allows for both qualitative and quantitative measurements in real time. The imaging provides visualization of the process in a qualitative sense, as seen by the contrast or brightness in the image. A dynamic process can be followed and visualized *in situ* as it occurs within the sample in real time. On the other hand, we have found that localized spectroscopy is necessary to get rigorous quantitative measurements, since the signal intensity in the volume element is directly related to the amount of both liquid oil and water in the sample. It was shown that for the simple triglyceride model systems used, the oil signal disappeared as the fat fully crystallized. Parallels between the images taken of the crystallization dynamics of the (40:60) trimyristin and the corresponding localized spectra at the center of the container is presented in Figure 6. The water peak in the emulsion served as the internal standard to ensure that any change in the oil peak could be assigned to crystallization and not to another phenomenon, such as an eventual creaming. The disappearance of the oil signal corresponding to complete fat crystallization in the emulsion followed a nonlinear curve.

Crystallization in specific spatial locations by localized spectroscopy. Localized spectroscopy of the trimyristin (40:60) emulsion using STE sequence as a function of time was performed in three different loca-

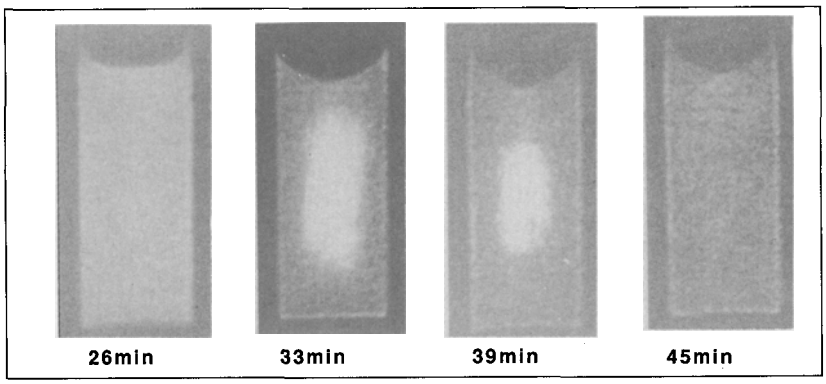

FIG. 5. Crystallization of a trimyristin emulsion: Images. Fat weighted images taken (left to right) at 21, 26, 33, 39 and 45 min are shown. Overall crystallization occurs suddenly in a 10-min time frame after approximately 30 min. It occurs from the edge to the center of the emulsion.

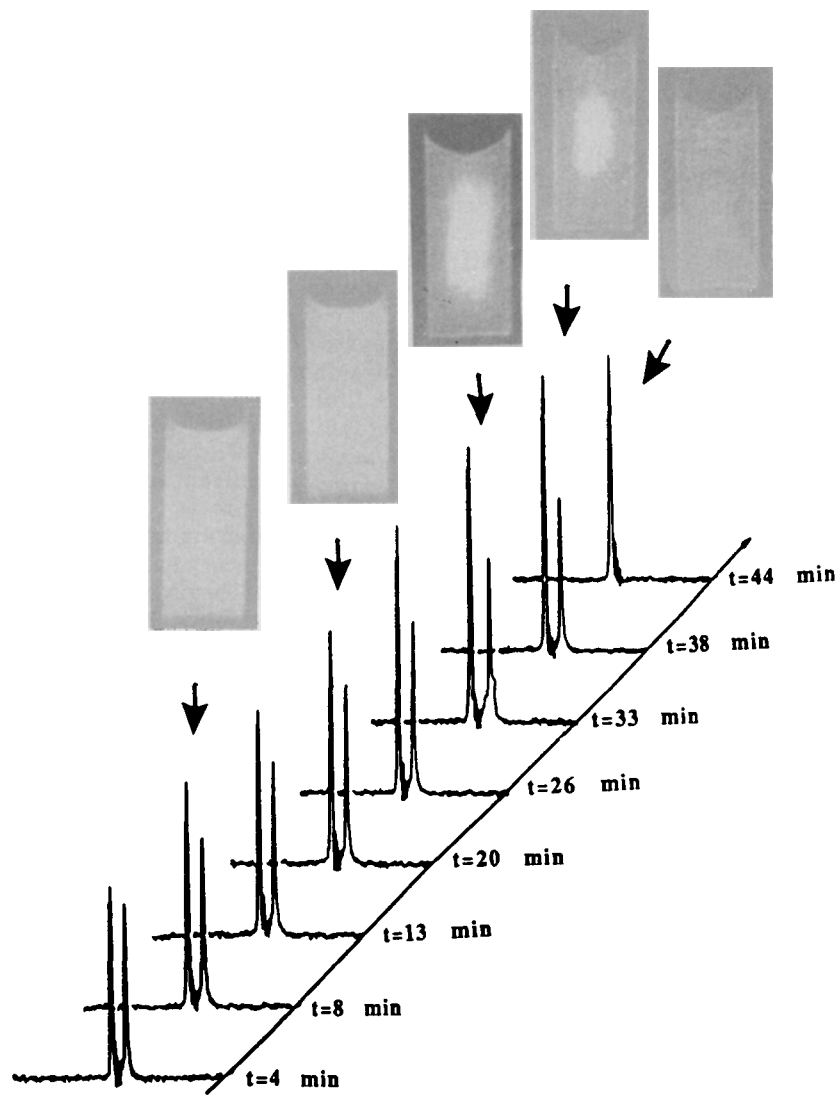

FIG. 6. Crystallization of trimyristin emulsion related to corresponding localized spectra at the center of the emulsion. Emulsion images and localized spectra are shown. Localized spectroscopy can follow crystallization patterns from the disappearance of the oil specifically at any location in a sample and for any volume element size. As localized spectroscopy is performed alternatively with imaging, the time frame can be accurately determined. Crystallization can be followed in real time.

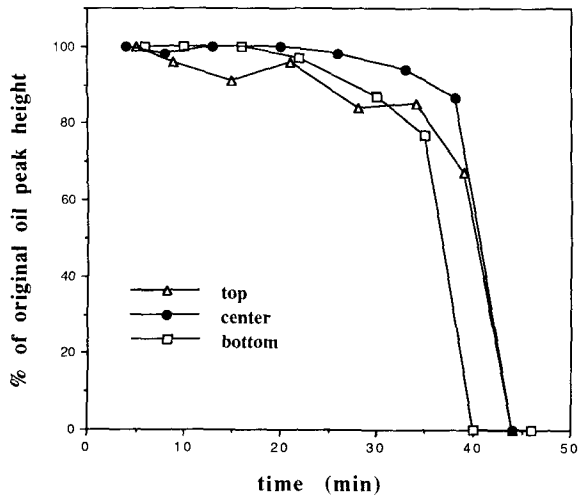

FIG. 7. Localized spectroscopy at the top, center and bottom of the trimyristin emulsion crystallizing. The disappearance of the oil peak corresponding to crystallization is quite sudden. A drop to no signal corresponding to complete crystallization occurs after 35 min (average), depending on the location in the sample. Crystallization tends to happen earlier at the top and bottom of the sample, but the crystallization pattern is a sigmoid type curve, fairly constant, whatever the location within the sample.

tions in the sample—at the top, bottom and center, respectively. As shown on Figure 7, spatial resolution of 0.064 mL volume-elements showed an abrupt disappearance of the oil signal corresponding to fat crystallization. A gradual decrease in oil signal occurred over the first 30–35 min, followed by a more rapid decline to no signal corresponding to complete crystallization. The crystallization patterns were relatively the same whatever the spatial location in the sample was, although it occurred earlier towards the top and bottom of the emulsion, showing again that crystallization in the emulsion occurred from the edge to the center of the emulsion, as illustrated by the images previously taken. Crystallization does not proceed throughout the emulsion as a whole, but rather is progressive from the edge to center. This reinforces the importance of localized spectroscopy to follow the crystallization process. Indeed, the average emulsion would have resulted in a broad or gradual crystallization pattern measurement, whereas localized spectroscopy showed that within any small volume, crystallization was quite rapid. The technique demonstrated that crystallization may very well seem a relatively slow process from an overall point of view, but that it occurs rapidly from location to location.

ACKNOWLEDGMENTS

The authors gratefully acknowledge the support of the California Dairy Foods Center, the Wisconsin Milk Marketing Board (grant #89-24) and the U.C. Davis NMR Facility.

REFERENCES

1. Tolboe, O., in *Milkfat and its Modification. Contribution at a Lipidoforum Symposium, Göteborg, January 26-27,* edited by R. Marcuse, Scandinavian Forum for Lipid Research and Technology, Göteborg, 1984, pp. 43–50.
2. Frede, E., D. Precht and H. Timmen, *Ibid.* pp. 37–42.
3. Hagemann, J.W., in *Polymorphism of Fats and Fatty Acids,* edited by N. Garti and K. Sato, Marcel Dekker Inc., New York, 1988, pp. 9–96.
4. Timms, R.E., *Aust. Dairy Technol. June,* 47 (1980).
5. Koyano, T., I. Hachiya, T. Arishima, K. Sato and N. Sagi, *J. Am. Oil Chem. Soc. 66*:675 (1989).
6. Broto, F., D. Clausse, L. Babin and M. Clausse, *Coll. and Polym. Sci. 257*:302 (1979).
7. Walstra, P., and E.C.H. van Beresteyn, *Neth. Milk Dairy J. 29*:35 (1975).
8. Söderberg, I., L. Hernqvist and W. Buchheim, *Milchwissenschaft 44*:403 (1990).
9. deMan, J.M., and M. Finoro, *Can. Inst. Food Sci. Technol. 13*:167 (1980).
10. Barfod, N.M., and N. Krog, *J. Am. Oil Chem. Soc. 64*:112 (1987).
11. German, J.B., and M.J. McCarthy, *J. Ag. and Food Chem. 37*:1321 (1989).
12. McCarthy, M.J., *AIChE Journal 36*:287 (1990).
13. Edelstein, W.A., J.M.S. Hutchison, G. Johnson and T.W. Redpath, *Phys. Med. Biol. 25*:751 (1980).
14. Frahm, J., K.D. Merboldt and W. Hanicke, *J. of Magnetic Resonance 72*:502 (1987).
15. Abragam, A., *The Principles of Nuclear Magnetism,* Clarendon Press, Oxford, 1961.
16. Valk, J., C. MacLean and P.R. Algra, *Basic Principles of Magnetic Resonance Imaging,* Elsevier Science Publishers, Amsterdam-New York-Oxford, 1985.
17. Morris, P.G., *Nuclear Magnetic Resonance Imaging in Medicine and Biology,* Clarendon Press, Oxford, 1986.
18. Winkler, M., M.J. McCarthy and J.B. German, *J. of Food Sci., submitted* for publication, 1990.
19. Sotak, C., *CSI Application Notes,* No. 861208 (1987).

[Received June 12, 1990; accepted November 3, 1990]